Lecture 2

Graded symplectic geometry and the HMS framework

Umut Varolgüneş
Mini lecture series, Kyoto University

1 Plan for the lectures

In Lecture 1 we discussed Floer theory on surfaces, the wrapped category of T^*S^1, and the HMS statements for the cylinder and the two-torus. This lecture supplies the geometric language needed in higher dimensions: graded symplectic manifolds, Liouville and Weinstein geometry, the symplectic structures associated to Calabi–Yau and log Calabi–Yau varieties, and large volume limit data. We then state the corresponding versions of HMS and discuss some examples in dimensions two and three.

We will name the relevant Fukaya categories without constructing them today. Lecture 3 will return to Lagrangian Floer theory, its absolute, wrapped, and relative versions, and then to Floer theory and Fukaya categories with support.

2 Graded symplectic geometry

2.1 Symplectic manifolds and Lagrangians

A *symplectic manifold* is a smooth manifold M^{2n} with a closed, nondegenerate two-form ω. Nondegeneracy means that $v \mapsto \omega(v, -)$ is an isomorphism $T_xM \to T_x^*M$ at every point. A symplectomorphism $\phi : (M_0, \omega_0) \to (M_1, \omega_1)$ is a diffeomorphism with $\phi^*\omega_1 = \omega_0$.

A submanifold $L \subset M$ is *Lagrangian* if

$$\dim L = n, \qquad \omega|_{TL} = 0.$$

We may also consider Lagrangian immersions $\iota : L \to M$, requiring $\iota^*\omega = 0$. Tangent-plane and brane data are then placed on the domain of the immersion, as in Lecture 1.

For a symplectic vector space (V, ω), its Lagrangian Grassmannian $\mathrm{Lag}(V)$ is the space of Lagrangian subspaces of V. After choosing a compatible complex structure and a unitary basis it is $U(n)/O(n)$. These spaces form a bundle

$$\mathrm{Lag}(TM) \longrightarrow M.$$

A Lagrangian immersion determines its Gauss map $x \mapsto d\iota(T_xL)$ into this bundle. A *Lagrangian polarization* is a section of the same bundle, namely a Lagrangian plane field on M.

2.2 The grading structure

Choose a compatible almost complex structure J: thus $g(v,w) = \omega(v, Jw)$ is a Riemannian metric. Its space of choices is contractible. Write $T^*_J M$ for the complex dual of (TM, J) and $K_M = \Lambda^n_{\mathbb{C}} T^*_J M$ for its complex determinant line bundle. To keep the orientation convention from Lecture 1, we choose a nowhere-zero smooth section Ω of K_M, up to homotopy. In a complex Calabi–Yau example, Ω can be holomorphic.

For a Lagrangian plane $\ell \subset T_x M$ and any real basis $v_1, \ldots, v_n$ of ℓ, define its squared phase by

$$\alpha(\ell) = \frac{\Omega(v_1, \ldots, v_n)^2}{|\Omega(v_1, \ldots, v_n)|^2} \in S^1. \tag{1}$$

This is independent of the basis, including its orientation. Pulling back $\mathbb{R} \to S^1$, $a \mapsto e^{2\pi i a}$, gives the Maslov cover

$$\widetilde{\mathrm{Lag}}(TM) = \{(\ell, a) : e^{2\pi i a} = \alpha(\ell)\}.$$

More generally, a trivialization of $K_M^{\otimes 2}$ suffices to define this cover, so $2c_1(M) = 0$ is the relevant obstruction to that choice. Our choice of Ω is stronger and also gives the orientation convention below.

A polarization η can also be used to define a grading structure [1, Examples 2.9–2.10]. Directly, define

$$\widetilde{\mathrm{Lag}}_\eta(T_x M) = \{(\ell, [\gamma]) : \gamma(0) = \eta_x,\ \gamma(1) = \ell\},$$

where γ is a path in $\mathrm{Lag}(T_x M)$ and homotopies fix its endpoints. Since $\pi_1(U(n)/O(n)) \cong \mathbb{Z}$, this is the universal cover of each fiber, with deck transformations indexed by $\mathbb{Z}$. These covers form a bundle over M, and a grading of a Lagrangian is a lift of its Gauss map to this bundle. The constant paths give η a distinguished lift. If η is oriented, it determines a homotopy class of volume forms Ω positive on η; the two constructions then agree. The path construction itself does not require η to be oriented.

2.3 Maslov zero and graded Lagrangians

For a Lagrangian L, the phase map is $\alpha_L(x) = \alpha(T_x L)$. Its class

$$\mu_L = \alpha_L^*[d\vartheta] \in H^1(L; \mathbb{Z}), \qquad S^1 = \mathbb{R}/\mathbb{Z},$$

is the Maslov class relative to the grading structure. A *grading* is a continuous lift $a_L : L \to \mathbb{R}$ with $e^{2\pi i a_L} = \alpha_L$. Such a lift exists exactly when $\mu_L = 0$. Thus Maslov zero is a condition, while a grading is a choice; on a connected L the choices form a $\mathbb{Z}$-torsor.

The grading orients L by declaring a basis positive when

$$e^{-\pi i a_L(x)} \Omega(v_1, \ldots, v_n) > 0.$$

The expression is real and nonzero by (1). Changing a_L by an odd integer reverses this orientation. In dimension one, normalize Ω to be positive on the oriented line field η. Then a_L is the lifted tangent angle in units of π, exactly as in Lecture 1. For transverse curves the degree remains $|x| = \lceil a_{L_1}(x) - a_{L_0}(x) \rceil$.

2.4 Spin structures and brane data

We use the orientation induced by the grading. A *spin structure* on an oriented n-manifold L is a lift of its oriented orthonormal frame bundle from $SO(n)$ to its double cover $\mathrm{Spin}(n)$. Thus it is a principal $\mathrm{Spin}(n)$-bundle P_{Spin} with an equivariant map to the frame bundle inducing

$$P_{\mathrm{Spin}}/\{\pm 1\} \cong P_{SO}(TL).$$

The choice of metric does not matter. A spin structure exists exactly when the second Stiefel–Whitney class vanishes:

$$w_2(TL) = 0 \in H^2(L; \mathbb{Z}/2).$$

When it exists, its isomorphism classes form a torsor for $H^1(L; \mathbb{Z}/2)$: after choosing one structure s, every other one is uniquely $s + \epsilon$ for some $\epsilon \in H^1(L; \mathbb{Z}/2)$ [2]. A grading does not supply a spin structure, and $c_1(M) = 0$ does not in general imply $w_2(TL) = 0$.

For S^1 there are two spin structures. The *bounding* one extends over the disk; the *nonbounding* one does not. In the double-cover description these are the connected and disconnected covers of S^1, respectively. A torus T^n has 2^n spin structures, while $\mathbb{R}^n$ has a unique one up to isomorphism. Thus the torus fibers and cotangent fibers appearing in these lectures are spin.

Why this enters Floer theory. Spin structures provide coherent orientations of the determinant lines of the linearized Cauchy–Riemann operators. Together with the usual orientation-line conventions for generators, these determine the signs of rigid strips and polygons, compatibly with gluing. They are therefore part of the data for the signed Floer constructions over $\mathbb{Z}$ and characteristic-zero coefficients. In characteristic two these signs disappear; see [3, §§1.2, 2.4]. For an immersed Lagrangian the spin structure, like the grading and local system, is placed on its domain.

Changing s to $s + \epsilon$ changes the sign of a disk in class $\beta \in \pi_2(M, L)$ by

$$(-1)^{\langle \epsilon, \partial\beta \rangle}.$$

This is also the holonomy of the rank-one sign local system ℓ_ϵ with $\mathrm{hol}_{\ell_\epsilon}(\gamma) = (-1)^{\langle \epsilon, [\gamma] \rangle}$. Accordingly, after identifying the generator orientation lines, changing the spin structure has the same effect on Floer operations as replacing a local system E by $E \otimes \ell_\epsilon$. On a circle this multiplies its holonomy by -1, explaining the spin/local-system convention used in Lecture 1.

More generally, one may fix a background class $b \in H^2(M; \mathbb{Z}/2)$ and use Lagrangians satisfying $w_2(TL) = \iota^* b$, equipped with *relative spin structures*. These are additional choices, not merely the equality of characteristic classes; see [4, §3] for the definition and the orientation-change formula. In the spin setup used here we take $b = 0$ and choose ordinary spin structures. Our brane data thus include a grading, a spin structure, and a local system, together with any required unobstructedness data.

3 Liouville and Weinstein geometry

3.1 Liouville manifolds, subdomains, and skeleta

Let $\omega = d\lambda$. The *Liouville vector field* Z is defined by

$$\iota_Z \omega = \lambda.$$

Cartan's formula gives $\mathcal{L}_Z\omega = \omega$ and $\mathcal{L}_Z\lambda = \lambda$. A *Liouville manifold* is a manifold X equipped with such a form λ, for which Z is complete. The finite-type manifolds used here are completions of compact Liouville domains, with cylindrical ends as described below.

A *Liouville subdomain* $W_0 \subset X$ is a compact codimension-zero submanifold, possibly with corners, on whose boundary faces Z points outward. Its completion is canonically embedded in X by continuing the Liouville flow; its image is

$$\widehat{W}_0 = \bigcup_{t\geq 0} \phi_Z^t(\operatorname{Int} W_0) \subset X.$$

One may round the corners to obtain a smooth boundary.

For a finite-type manifold we can choose W_0 so that its completion is all of X. On the end, Liouville flow gives coordinates $[0,\infty) \times Y$, where $Y = \partial W_0$, in which

$$\lambda = e^r\alpha, \qquad \alpha = \lambda|_Y, \qquad Z = \partial_r.$$

Here α is a contact form on Y.

The *skeleton* consists of the points that do not escape under positive Liouville flow:

$$\operatorname{Skel}(X,\lambda) = \{x \in X : \{\phi_Z^t(x) : t \geq 0\} \text{ is relatively compact}\}.$$

For a Liouville domain W_0, its skeleton is $\bigcap_{t\geq 0} \phi_Z^{-t}(W_0)$.

3.2 The Weinstein condition

A *Lyapunov function* for a Liouville structure is an exhausting smooth function φ for which Z is gradient-like: for some Riemannian metric and a positive function δ,

$$d\varphi(Z) \geq \delta\big(|Z|^2 + |d\varphi|^2\big).$$

If a Liouville structure admits a *Morse* Lyapunov function, it is called *Weinstein*. In the finite-type case φ has only finitely many critical points. Their stable manifolds are isotropic, so their Morse indices are at most n, and their union is the skeleton. See [6, §§1.1, 3.1].

For closed Q, the tautological form $\lambda = p\,dq$ gives a Liouville structure on T^*Q. To write down a Morse Lyapunov function, choose a Riemannian metric on Q and a Morse function $f : Q \to \mathbb{R}$. Set

$$H(q,p) = p(\nabla f(q)), \qquad \lambda_\epsilon = \lambda - \epsilon\, dH, \qquad \varphi_\epsilon(q,p) = \frac{1}{2}|p|^2 + \epsilon f(q).$$

Here $d\lambda_\epsilon = d\lambda$. In the horizontal–vertical splitting from the metric, its Liouville field is

$$Z_\epsilon = (\epsilon\nabla f,\ p - \epsilon(\nabla^2 f)^* p),$$

and

$$d\varphi_\epsilon(Z_\epsilon) = |p|^2 - \epsilon \operatorname{Hess} f(p^\sharp, p^\sharp) + \epsilon^2 |df|^2.$$

For sufficiently small $\epsilon > 0$ this satisfies the gradient-like inequality. The function φ_ϵ is exhausting and Morse, with critical points $(q,0)$ for $q \in \operatorname{Crit}(f)$, and Z_ϵ is complete. This gives the desired Weinstein perturbation. The path $\lambda_t = \lambda - t\epsilon\, dH$ is outward pointing on a fixed sphere bundle for all $t \in [0,1]$. Thus it gives a Liouville deformation as in §3.4; the perturbation preserves the strongly exact symplectomorphism type of T^*Q.

3.3 Exactness and conicity

A Lagrangian immersion is *exact* if

$$\iota^*\lambda = df_L.$$

The function f_L is its primitive. A proper Lagrangian is *conical* at infinity if it is invariant under the Liouville flow outside a compact set. On a cylindrical end it is of the form $[r_0, \infty) \times \Lambda_L$, where Λ_L is Legendrian in the contact boundary.

Indeed, if Z is tangent to L, then $\lambda|_{TL} = \omega(Z, -)|_{TL} = 0$. Consequently an exact conical Lagrangian has a primitive constant on each end. Different ends may have different constants.

We call a symplectomorphism *strongly exact* if

$$\phi^*\lambda_1 - \lambda_0 = dF, \qquad F \in C_c^\infty(X_0). \tag{2}$$

Thus it preserves the Liouville forms near infinity. The map ϕ itself need not be compactly supported. Requiring a compactly supported primitive F is part of this definition.

3.4 Liouville deformation equivalence

For the finite-type manifolds in these lectures, we define deformations using compact domains. A *Liouville deformation* on a fixed compact manifold W with boundary is a smooth family of one-forms λ_t, $0 \le t \le 1$, such that $d\lambda_t$ is symplectic and its Liouville field Z_t points strictly outward along ∂W for every t. The symplectic form is allowed to vary.

Two finite-type Liouville manifolds are *deformation equivalent* if they are the completions of the endpoints of such a family, allowing identifications by diffeomorphisms and finite concatenations of families. Using the Liouville collars to identify the completions, we obtain a family on one open manifold with a common end

$$[0, \infty) \times Y, \qquad \lambda_t = e^r \alpha_t,$$

where α_t is a smooth family of contact forms on the compact manifold Y. This control at infinity is part of the definition: pointwise completeness of a family of Liouville fields alone does not supply it.

The Moser argument. Deformation-equivalent finite-type Liouville manifolds are strongly exact symplectomorphic. Here is the argument on the identified completions. Define the time-dependent vector field V_t by

$$\iota_{V_t} d\lambda_t = -\dot\lambda_t.$$

On the cylindrical end, both sides scale by e^r, so V_t is translation invariant in r. Its coefficients are uniformly bounded on $[0, 1] \times Y$; consequently its flow Φ_t exists throughout $0 \le t \le 1$. Moreover, on the end,

$$\lambda_t(V_t) = d\lambda_t(\partial_r, V_t) = \dot\lambda_t(\partial_r) = 0.$$

Cartan's formula now gives

$$\frac{d}{dt}\Phi_t^*\lambda_t = \Phi_t^*(\dot\lambda_t + \iota_{V_t} d\lambda_t + d(\lambda_t(V_t))) = d\big(\Phi_t^*(\lambda_t(V_t))\big).$$

Integrating, we obtain

$$\Phi_1^*\lambda_1 - \lambda_0 = dF, \qquad F = \int_0^1 \Phi_t^*(\lambda_t(V_t))\, dt \in C_c^\infty(X). \tag{3}$$

Indeed, the integrand vanishes sufficiently far out, uniformly in t, and the flow has bounded radial displacement there. Thus the *function* F has compact support, as required in (2). Differentiating (3) also gives $\Phi_1^* d\lambda_1 = d\lambda_0$. This is the finite-type Liouville version of Moser stability; see also [7, §11.2].

What this preserves. If $\lambda_0|_L = df_L$, then the primitive on $\Phi_1(L)$, pulled back to L, is $f_L + F|_L$. Near infinity Φ_1 preserves the Liouville forms and intertwines their Liouville fields, so conical Lagrangians remain conical. Gradings and the other brane data can be transported along the deformation. The skeleton can change during a deformation; it need not be carried to the new skeleton by Φ_1.

This principle justifies changing the cotangent bundle perturbation in §3.2, rounding a Liouville boundary, and moving a truncation boundary through the cylindrical end. Below we also use it to remove auxiliary choices in the affine and ray diagram constructions, after producing the required Liouville deformation.

4 Symplectic geometry from algebraic geometry

4.1 Smooth affine varieties

Let X be a smooth affine variety over $\mathbb{C}$. Choose a closed algebraic embedding $X \hookrightarrow \mathbb{C}^N$ and restrict

$$\varphi = \frac{1}{4}\sum_{j=1}^{N} |z_j|^2, \qquad \lambda = -d\varphi \circ J, \qquad \omega = d\lambda.$$

After a small Morse perturbation and completion of a sufficiently large regular sublevel, the associated Weinstein manifold is well-defined up to strongly exact symplectomorphism [5, §4b]. The geometric input is that the choices of algebraic embedding and exhaustion give deformation-equivalent Liouville domains. The Moser argument in §3.4 then gives the strongly exact identification of their completions.

If K_X is trivial, choose a nowhere-zero algebraic volume form Ω. Together with the Kähler structure it gives the grading data from Section 2. The form Ω, or its homotopy class, is part of the data when the grading matters.

4.2 Log Calabi–Yau pairs and their boundary complexes

The log Calabi–Yau pairs used here are smooth projective pairs $(\overline{X}, D_\infty)$ with reduced simple normal crossing boundary

$$D_\infty = \sum_i D_i, \qquad K_{\overline{X}} + D_\infty \sim 0.$$

Equivalently, there is a meromorphic volume form with a simple pole along each boundary component and no other zeros or poles. On $X = \overline{X} \setminus D_\infty$ it becomes a nowhere-zero holomorphic volume form. We will mainly use examples in which X is affine. Affineness and the log Calabi–Yau condition are separate requirements. Thus an affine log Calabi–Yau variety determines a graded Weinstein manifold.

The *dual intersection complex* of D_∞ records its strata: a vertex for each component, an edge for each connected component of a double intersection, and a k-simplex for each connected component of an intersection of $k+1$ distinct components. The face maps come from inclusions of strata. We call the boundary *maximally degenerate* if this complex has dimension $\dim_{\mathbb{C}} X - 1$.

Theorem 4.1 (Independence of compactification)**.** *Suppose X admits two smooth projective log Calabi–Yau compactifications $(\overline{X}_1, D_{\infty,1})$ and $(\overline{X}_2, D_{\infty,2})$ with reduced simple normal crossing boundaries. Their dual intersection complexes are PL-homeomorphic. In particular, the underlying topological space and its dimension are independent of the compactification.*

This follows from the invariance of the dual complex under crepant birational maps [8, Proposition 11].

Is the dual complex a manifold? For maximally degenerate smooth log Calabi–Yau pairs in complex dimensions two and three, it is respectively S^1 and S^2 [26, §33]. More generally, under our simple normal crossing hypotheses the maximally degenerate dual complex is homeomorphic to S^{n-1} for $n \leq 5$. Without maximal degeneration, even a boundary can occur: two transverse smooth quadrics in $\mathbb{P}^3$ form an anticanonical divisor with dual complex an interval. A smooth connected anticanonical divisor gives a point. In arbitrary dimension a log Calabi–Yau dual complex need not be a manifold, even allowing boundary.[1]

For a smooth projective toric variety and its toric boundary, the complement is $(\mathbb{C}^*)^n$, with volume form

$$\Omega = \frac{dz_1}{z_1} \wedge \cdots \wedge \frac{dz_n}{z_n}.$$

The dual complex is an $(n-1)$-sphere.

Definition 4.2 (Generalized toric model)**.** *Let X be an affine log Calabi–Yau variety of complex dimension n. A* generalized toric model *of X is a presentation $X \cong Y \setminus D$ obtained as follows:*

(i) Start with a smooth projective toric n-fold Y_0 and its toric boundary D_0.
(ii) Deform D_0 within the anticanonical linear system to a reduced simple normal crossing divisor D_1, allowing some of the boundary crossings to be smoothed.
(iii) Perform a sequence of blowups along smooth codimension-two centers. At each step the center lies in one boundary component, is not contained in any other component, and meets the remaining boundary with normal crossings. Use the strict transform of the boundary after each blowup, obtaining (Y, D).

The choices and sequence of operations are part of the model. If step (ii) is omitted, we call it a toric model*.*

Exercise 3 (a log Calabi–Yau modification). Let $(\overline{X}, D_\infty)$ be a smooth log Calabi–Yau pair and let $Z \subset D_1$ be a smooth codimension-two center, not contained in any other boundary component and meeting the remaining boundary with normal crossings. Blow up Z, with exceptional divisor E, and use only the strict transform $\widetilde{D}_\infty$ as the new boundary. Prove

$$K_{\widetilde{X}} + \widetilde{D}_\infty = \pi^*(K_{\overline{X}} + D_\infty),$$

and hence that $\widetilde{X} \setminus \widetilde{D}_\infty$ is log Calabi–Yau.

For all exercises: You are welcome to use the literature, but the writeup and explanations must be your own.

[1] For a non-affine example, let E be an elliptic curve and $\tau \neq 0$ a point of order two. On $(\mathbb{P}^1)^5 \times E$ let g invert the first four $\mathbb{P}^1$ coordinates, fix the fifth, and translate E by τ. The quotient is smooth projective and the image of the toric boundary times E is simple normal crossing. The logarithmic volume form is g-invariant, so the pair is log Calabi–Yau. Its dual complex is $S^4/\operatorname{diag}(-1,-1,-1,-1,1) = \operatorname{Susp}(\mathbb{RP}^3)$, which is not a manifold at its two suspension points. This pair is not maximally degenerate.

4.3 Compact Kähler manifolds and adjunction

A compact complex manifold together with a Kähler class determines a symplectic manifold up to symplectomorphism. Indeed, if ω_0 and ω_1 represent the same class, then $\omega_t = (1-t)\omega_0 + t\omega_1$ is a path of cohomologous Kähler forms, and Moser's argument supplies a symplectomorphism. Every smooth complex submanifold inherits a Kähler form. A general real Kähler class need not be integral. If the class is integral, it is the first Chern class of a positive line bundle, and Kodaira's embedding theorem makes the compact complex manifold projective.

The toric case. A compact symplectic toric manifold of real dimension $2n$ carries an effective Hamiltonian action of T^n. Its moment map $\mu : M \to \mathfrak{t}^*$ records the Hamiltonians of the circle subgroups; its image is a *Delzant polytope* P. This means that exactly n facets meet at each vertex and their primitive integral inward normals form a basis of the torus lattice. The inverse image of a point in the interior is a Lagrangian n-torus. Over the relative interior of a codimension-k face, k circle directions collapse, leaving an $(n-k)$-torus; vertices therefore correspond to fixed points. The inverse image of an edge is a symplectic two-sphere, and its area is the integral affine length of that edge, when circle parameters have period one. Thus the polytope records both the orbit strata and the symplectic areas. For an integral Kähler class, choose the additive normalization of μ so that the vertices lie in the character lattice; P is then a lattice polytope.

Adjunction says that for a smooth complex submanifold $Y \subset M$,

$$K_Y \cong K_M|_Y \otimes \det N_{Y/M}.$$

In particular, a smooth anticanonical divisor has trivial canonical bundle. A degree-d hypersurface $Y \subset \mathbb{P}^N$ has

$$K_Y \cong \mathcal{O}_Y(d-N-1).$$

This gives the cubic elliptic curve, the quartic K3 surface, and the quintic Calabi–Yau threefold. The complement of a smooth anticanonical divisor in a projective variety is log Calabi–Yau; when the divisor is ample, the complement is affine.

5 Large volume limit data

5.1 Symplectic divisors and adapted primitives

Let $D = \bigcup_{i=1}^N D_i$ be a symplectic simple normal crossing divisor: the D_i are transversely intersecting symplectic submanifolds of real codimension two, every intersection $D_I = \bigcap_{i\in I} D_i$ is symplectic, and the intersection orientation on D_I agrees with its symplectic orientation. Here the intersection orientation is defined by the oriented normal-bundle identification

$$N_M D_I \cong \bigoplus_{i\in I} N_M D_i|_{D_I}.$$

This is the orientation compatibility condition; it is required for every nonempty intersection [27, Definition 2.1].

For the purposes of these lectures, *large volume limit data* includes positive weights a_i and an adapted primitive θ on $M \setminus D$ such that

$$d\theta = \omega|_{M\setminus D}, \qquad [\omega] = \sum_i a_i \,\mathrm{PD}[D_i]. \tag{4}$$

The residue convention is

$$\lim_{\epsilon\to 0}\int_{\gamma_{i,\epsilon}}\theta = -a_i,$$

where $\gamma_{i,\epsilon}$ is a small positively oriented meridian. For example, with angular coordinate $\vartheta_i \in \mathbb{R}/\mathbb{Z}$ and normal area coordinate ρ_i, the normal part of the primitive is $(\rho_i - a_i)d\vartheta_i$. Existence of the adapted primitive and the required convexity of the complement are included in the data.

For a compact oriented surface S mapped by u into M, transverse to D and with $u(\partial S) \subset M\setminus D$, Stokes' theorem on the punctured surface gives

$$\int_S u^*\omega - \int_{\partial S} u^*\theta = \sum_i a_i(u\cdot D_i). \tag{5}$$

The small boundary circles of the punctured domain have the opposite orientation to positive meridians, which accounts for the sign. The expression $u \cdot D$ in the handwritten shorthand denotes this weighted intersection number.

If $L \subset M \setminus D$ satisfies $\theta|_L = df_L$, the boundary term vanishes for a disk with boundary on L. For polygons on several exact Lagrangians, it is expressed by differences of the primitives at their corners. Formula (5) then relates the ordinary area weights to the divisor weights.

5.2 The affine setting and behavior at infinity

For a Liouville manifold (X, λ) coming from a compactification $(\overline{X}, D_\infty)$, we use an auxiliary divisor $D \subset X$ and a primitive λ_D on $X \setminus D$ adapted to its weights. The compactification boundary D_∞ and the auxiliary divisor D play different roles. In the compactification picture choose λ_D with residue zero around each component of D_∞ and prescribed negative residue $-a_i$ around each component D_i of D:

$$\lim_{\epsilon\to 0}\int_{\gamma_{\infty,j,\epsilon}}\lambda_D = 0, \qquad \lim_{\epsilon\to 0}\int_{\gamma_{i,\epsilon}}\lambda_D = -a_i, \qquad a_i > 0.$$

All meridians are positively oriented. Existence of this primitive, the analogues of (4)–(5), and the appropriate cohomological condition are part of the data.

We assume that D is cylindrical and is preserved by the local S^1-actions near D_∞. These actions rotate the normal directions to the components of the compactification boundary. This makes the divisor compatible with the wrapping used below. Removing D, choosing the adapted primitive, and completing produces the complement geometry denoted by $(X \setminus D, \lambda_D)$. Changes of the adapted data through a family with the same prescribed residues and a uniformly convex end give strongly exact isomorphic completions by §3.4. Such a family must be checked when using this independence of choices.

For $X = \mathbb{C}^*$ and a single point $D = \{1\}$, the following picture shows an exhausting Weinstein model of $X \setminus D$. We draw $\mathbb{C}^*$ as a cylinder, with its two ends corresponding to 0 and ∞.

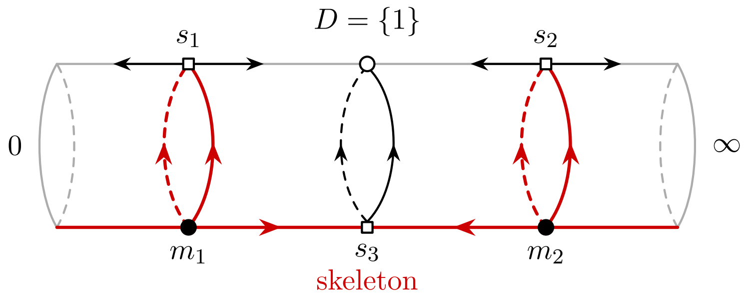

The dots m_1, m_2 are minima; the squares s_1, s_2, s_3 are saddles. Arrows show positive Liouville flow: along the red skeleton toward the saddles, and along the black unstable branches away from them. Dashed arcs lie on the back of the cylinder.

6 The categories and their coefficient rings

6.1 Absolute and relative theories

We now name the categories, deferring their construction to Lecture 3. We use suitable graded, spin branes with local systems as in §2.4, and take the unobstructed versions of the theories. Let $\Lambda = \Lambda_{\mathbb{Q}}$ be the Novikov field from Lecture 1, with $\mathrm{val}(T^a) = a$.

For a closed graded symplectic manifold, the absolute category is $\mathrm{Fuk}(M)$ over Λ. With large volume limit data we have a relative category with formal parameters:

$$\mathrm{Fuk}(M, D) \quad \text{over} \quad \Bbbk[[Q_1, \ldots, Q_N]].$$

Its objects are the chosen compact θ-exact branes in $M \setminus D$, with the required unobstructedness data. Here $\Bbbk = \mathbb{Z}$ in the integral constructions under consideration; one can extend coefficients to $\mathbb{Q}$. A polygon contributes the weight

$$Q_1^{u \cdot D_1} \cdots Q_N^{u \cdot D_N}.$$

Divisor-compatible holomorphic curves have nonnegative intersections. The completion permits infinitely many terms with increasing total intersection number. The map

$$Q_i \longmapsto T^{a_i} \tag{6}$$

converges because $a_i > 0$. By (5), rescaling Floer generators by the boundary-action terms converts these monomial weights into the absolute area weights. A precise relative construction is discussed in [9].

For a graded Liouville manifold, the exact wrapped category is $\mathcal{W}(X)$ over $\mathbb{Z}$. A strongly exact symplectomorphism, with the brane data transported, induces an equivalence of wrapped categories. Thus §3.4 lets us use any representative of the same finite-type Liouville deformation class. For a relative category the divisor data must also be transported. Its relative version in the finite-count model is

$$\mathcal{W}(X, D) \quad \text{over} \quad \mathbb{Z}[Q_1, \ldots, Q_N].$$

We choose branes disjoint from D whose exactness is compatible with both λ and λ_D. The polynomial model assumes finiteness of the relevant counts for fixed inputs, as provided by the exactness and compactness setup in the examples. This permits the specialization $Q_i = 1$, which forgets the intersection weights. Recovering the full absolute category also requires that the chosen branes generate it. These comparison and generation assertions are part of the HMS picture below.

We often abbreviate the collection of parameters by Q. Evaluation at $Q = 1$ is used only for the polynomial model. Arbitrary formal power series in Q cannot be evaluated there.

6.2 The specialization at zero

Setting every $Q_i = 0$ retains precisely the curves disjoint from D. It initially retains the same objects. In the compact setting this gives the exact compact complement category

$$\mathrm{Fuk}^{\mathrm{cpt}}(M \setminus D, \theta)$$

on the chosen branes. Passing to its perfect completion allows us to use a generating collection in place of all such objects.

In the affine setting we write the corresponding category as

$$\mathcal{W}^{D\text{-away}}(X \setminus D, \lambda_D).$$

The superscript records the branes and wrapping inherited from the relative problem: objects come from X and stay away from D. This is followed by a separate enlargement to the full category

$$\mathcal{W}(X \setminus D, \lambda_D),$$

which allows admissible objects approaching the new ends created by removing D. Similarly, $\mathrm{Fuk}^{\mathrm{cpt}}(M \setminus D, \theta)$ and $\mathcal{W}(M \setminus D, \theta)$ have different allowed objects.

The primitive matters in these comparisons: being λ-exact and disjoint from D does not by itself imply λ_D-exactness. The compatibility of the branes with the adapted primitive is included in our setup. In categorical specialization statements, tensor products are understood in the derived sense.

7 The kinds of spaces appearing on the B-side

7.1 The mirror chart

The following table is the intended form of the mirrors in our examples. It records the difference between absolute geometry and geometry with large volume limit data.

A-side	Absolute mirror	With large volume limit data	Geometry
X affine	Scheme over $\mathbb{Z}$	Scheme over $\mathbb{Z}[Q]$	Nonproper
M compact	Rigid analytic space over $\Lambda_{\mathbb{Q}}$	Formal scheme over $\mathbb{Z}[[Q]]$	Proper

An affine A-side need not have an affine mirror. In the projective compact examples, the rigid analytic mirror can be the analytification of a projective variety. This is additional algebraic structure on the mirror.

7.2 Algebraic, formal, and analytic local models

An affine algebraic chart over a field $\Bbbk$ has the form

$$\mathrm{Spec}\,\frac{\Bbbk[x_1, \dots, x_k]}{(f_1, \dots, f_\ell)}.$$

Its points are prime ideals, with the Zariski topology and the usual structure sheaf. Schemes are obtained by gluing such affine charts (and the same definition works over a general base ring).

Set $R = \Lambda_{\mathbb{Q},\geq 0}$. Equip it with the valuation topology, equivalently the topology defined by powers of T. The ring $R\langle x_1, \ldots, x_k\rangle$ consists of *restricted* power series: their coefficients tend to zero in this topology. An admissible formal chart has the form

$$\operatorname{Spf} \frac{R\langle x_1, \ldots, x_k\rangle}{(f_1, \ldots, f_\ell)},$$

with an adically closed ideal and a topologically finitely presented, R-flat coordinate ring. Its points are the open prime ideals, that is, the prime ideals containing an ideal of definition. Its structure sheaf remembers all infinitesimal thickenings, not just the special fiber.

The corresponding rigid analytic chart is

$$\operatorname{Sp} \frac{\Lambda_{\mathbb{Q}}\langle x_1, \ldots, x_k\rangle}{(f_1, \ldots, f_\ell)}.$$

In the classical description its points are maximal ideals, with Tate's admissible G-topology. The algebra is a Tate algebra quotient; these charts glue to rigid analytic spaces. Berkovich spaces provide another way to package the associated analytic geometry. See [10].

For a formal family $\mathcal{Y}$ over $\mathbb{Z}[[Q]]$, apply (6), take the completed base change to R, and then take its rigid generic fiber to obtain the absolute mirror Y. If the formal family has a proper algebraic model, this agrees with the analytification of its generic fiber. In that case proper GAGA identifies the coherent theories. Algebraization is an extra assertion; the rigid generic fiber itself does not require it.

7.3 Coherent sheaves, perfect complexes, and Morita equivalence

In the HMS formulas, write

$$\operatorname{Coh}^{\mathrm{dg}}(Y) \quad \text{for an enhancement of } D^b \operatorname{Coh}(Y).$$

Here is a dg-localization definition. Let $C^b_{\mathrm{dg}}(\operatorname{Coh} Y)$ be the dg category of bounded complexes of coherent sheaves, with morphism complexes

$$\operatorname{Hom}^r(E, F) = \prod_i \operatorname{Hom}_{\mathcal{O}_Y}(E^i, F^{i+r}), \qquad d(f) = d_F f - (-1)^r f d_E.$$

Let W be its closed degree-zero quasi-isomorphisms. Define

$$\operatorname{Coh}^{\mathrm{dg}}(Y) := C^b_{\mathrm{dg}}(\operatorname{Coh} Y)[W^{-1}]_{\mathrm{dg}}.$$

This localization is universal, up to homotopy, for dg functors making the maps in W invertible in the homotopy category. Equivalently it is the derived dg quotient by the full dg subcategory of acyclic complexes:

$$C^b_{\mathrm{dg}}(\operatorname{Coh} Y)/\operatorname{Ac}^b_{\mathrm{dg}}(Y).$$

In the quotient model one makes each acyclic object A contractible by adjoining a degree--1 endomorphism h_A with $dh_A = \mathrm{id}_A$; over a general coefficient ring one first takes an appropriate homotopically flat replacement. Its homotopy category is $H^0 \operatorname{Coh}^{\mathrm{dg}}(Y) = D^b \operatorname{Coh}(Y)$; see [28]. The category $\operatorname{Perf}(Y)$ is the full dg subcategory of complexes locally quasi-isomorphic to bounded complexes of finite-rank locally free sheaves.

On a smooth mirror of the type considered here, bounded coherent complexes are perfect, so

$$\mathrm{Coh}^{\mathrm{dg}}(Y) \simeq \mathrm{Perf}(Y).$$

On a singular special fiber these categories generally differ. For example, a skyscraper sheaf at a singular point need not have a finite locally free resolution. This distinction is central to the following HMS chart.

An equivalence $\mathcal{C} \simeq_{\mathrm{Morita}} \mathcal{D}$ means an equivalence of their perfect completions:

$$\mathrm{Perf}_{A_\infty}(\mathcal{C}) \simeq \mathrm{Perf}_{A_\infty}(\mathcal{D}).$$

Thus we allow finite twisted complexes and split idempotents, as in Lecture 1. Taking homotopy categories gives the corresponding equivalence of split-closed derived categories.

8 The HMS conjectural picture

These are the proposed compatible equivalences for the geometric setups under consideration. They are a framework for the examples, not an existence theorem for a mirror to every graded symplectic manifold. The categories use the admissibility and coefficient conventions just described. The mirror families are assumed flat over their parameter rings, so their derived specializations agree with the ordinary fibers appearing below.

8.1 The compact setting

Let $\mathcal{Y}$ be the formal mirror with large volume limit data, let $\mathcal{Y}_0$ be its fiber at $Q = 0$, and let Y be its rigid generic fiber after (6). The picture is

$$\begin{aligned}
\mathrm{Fuk}(M) &\simeq_{\mathrm{Morita}} \mathrm{Coh}^{\mathrm{dg}}(Y) \simeq \mathrm{Perf}(Y),\\
\mathrm{Fuk}(M, D) &\simeq_{\mathrm{Morita}} \mathrm{Perf}(\mathcal{Y}),\\
\mathrm{Fuk}^{\mathrm{cpt}}(M \setminus D, \theta) &\simeq_{\mathrm{Morita}} \mathrm{Perf}(\mathcal{Y}_0),\\
\mathcal{W}(M \setminus D, \theta) &\simeq_{\mathrm{Morita}} \mathrm{Coh}^{\mathrm{dg}}(\mathcal{Y}_0).
\end{aligned}$$

The last two lines should intertwine the inclusion of compact objects into the wrapped category with the inclusion $\mathrm{Perf}(\mathcal{Y}_0) \subset \mathrm{Coh}^{\mathrm{dg}}(\mathcal{Y}_0)$. For a singular central fiber this inclusion can be proper. The torus and Tate curve from Lecture 1 illustrate this pattern.

8.2 The affine setting

Now let $\mathcal{Y} \to \mathrm{Spec}\,\mathbb{Z}[Q]$ be the relative mirror, and put $Y = \mathcal{Y}_1$ and $\mathcal{Y}_0 = \mathcal{Y}|_{Q=0}$, with all parameters respectively equal to one and zero. The analogous picture is

$$\begin{aligned}
\mathcal{W}(X) &\simeq_{\mathrm{Morita}} \mathrm{Coh}^{\mathrm{dg}}(Y) \simeq \mathrm{Perf}(Y),\\
\mathcal{W}(X, D) &\simeq_{\mathrm{Morita}} \mathrm{Perf}(\mathcal{Y}),\\
\mathcal{W}^{D\text{-away}}(X \setminus D, \lambda_D) &\simeq_{\mathrm{Morita}} \mathrm{Perf}(\mathcal{Y}_0),\\
\mathcal{W}(X \setminus D, \lambda_D) &\simeq_{\mathrm{Morita}} \mathrm{Coh}^{\mathrm{dg}}(\mathcal{Y}_0).
\end{aligned}$$

Again the passage from the third line to the fourth is an enlargement of the object class, reflected by perfect versus coherent complexes on the special fiber. Compatibility with specialization and the generation statements are part of this conjectural package.

For a broader framework combining these kinds of structures, we recommend Seidel's theory of *noncommutative Lefschetz pencils*; see [11, §§1b–1c]. It organizes more than the individual equivalences written above. We will use the chart here without developing that theory.

9 Examples and models in dimensions two and three

Here dimension means complex dimension, or half the real symplectic dimension. A regular Lagrangian torus fibration has a base with an integral affine structure: locally there are action coordinates whose transition maps lie in $\mathrm{GL}(n,\mathbb{Z}) \ltimes \mathbb{R}^n$. The *discriminant locus* $\Delta \subset B$ is the set of critical values, so over $B \setminus \Delta$ the fibration is a smooth torus bundle. Transport around a loop in $B \setminus \Delta$ acts on $H_1(T^n;\mathbb{Z})$ by an integral matrix: nontrivial monodromy obstructs a global basis of fiber cycles and appears dually in the linear parts of the affine coordinate changes.

9.1 The affine surface and a focus–focus singularity

A basic model linking affine modification and a nodal torus fibration is

$$U = \{uv = z-1\} \subset \mathbb{C}^2 \times \mathbb{C}^* \cong \mathbb{C}^2 \setminus \{uv = -1\}.$$

It is the modification of $\mathbb{A}^1_u \times \mathbb{G}_{m,z}$ with center $(u, z-1)$ and divisor $u = 0$. Its volume form is

$$\Omega = \frac{du}{u} \wedge \frac{dz}{z} = \frac{du \wedge dv}{z}.$$

The second expression shows directly that it extends without zeros across $u = 0$.

For the standard invariant Kähler form, the functions

$$\pi(u,v,z) = \left(\log|z|, \frac{|u|^2 - |v|^2}{2}\right)$$

Poisson commute. The second is a moment map, up to the Hamiltonian sign convention, for the circle action $(u,v,z) \mapsto (e^{it}u, e^{-it}v, z)$. The regular fibers are Lagrangian two-tori, and the fiber over $(0,0)$ is a nodal torus. The monodromy around the focus–focus value is conjugate to

$$\begin{pmatrix} 1 & 1 \\ 0 & 1 \end{pmatrix}.$$

This is the elementary singularity entering almost toric pictures of affine log Calabi–Yau surfaces. Toric models and the modifications above explain why toric regions and such local singularities occur together.

Exercise 4 (Duistermaat's fibration on T^*S^2). Consider a spherical pendulum of mass $m > 0$ and length $\ell > 0$, with $g > 0$. Give the round sphere $S^2_\ell \subset \mathbb{R}^3$ its induced metric, and identify cotangent vectors with tangent vectors, so that

$$T^*S^2_\ell = \{(q,p) \in \mathbb{R}^3 \times \mathbb{R}^3 : |q| = \ell,\ q \cdot p = 0\}.$$

Use the tautological form $\lambda = p \cdot dq$ and $\omega = d\lambda$. For every parameter $c \geq 0$, let

$$H_c(q,p) = \frac{|p|^2}{2m} + c\,mgh(q), \qquad h(q) = q_3, \qquad J(q,p) = q_1p_2 - q_2p_1.$$

Here h is height measured from the equatorial plane and J is the vertical angular momentum. The energy–momentum map

$$F_c = (J, H_c) : T^*S^2_\ell \longrightarrow \mathbb{R}^2_{(j,E)}$$

is Duistermaat's spherical-pendulum example [12].

(i) Show that J generates rotations about the vertical axis, that $\{J, H_c\} = 0$, and that F_c is proper. Show that its nonempty regular fibers are Lagrangian two-tori.

(ii) For every $c \geq 0$, determine the image and the critical values of F_c, and draw the bifurcation diagram. Describe $F_c^{-1}(j, E)$ for *every* point $(j, E) \in \mathbb{R}^2$, including empty fibers, boundary fibers, and exceptional fibers. Give their topology and identify the critical points of F_c on each fiber. Treat $c = 0$ explicitly, including the fiber over $(0, 0)$.

(iii) For $c > 0$, prove that the monodromy of the local system $H_1(F_c^{-1}(j, E); \mathbb{Z})$ is nontrivial around a small loop of regular values encircling $(0, cmg\ell)$, the value of the upright equilibrium. Explain what happens to the fibration and its monodromy when $c = 0$.

Hint (Cushman's argument). For $c > 0$, compare the regular energy hypersurfaces just below and just above the energy $cmg\ell$ of the upright equilibrium. Use Morse theory and identify the high-energy hypersurfaces by radial rescaling in the cotangent fibers. View these hypersurfaces as preimages of arcs in the base with endpoints on its boundary. What would trivial monodromy imply about their topology? See [13, §3.1].

9.2 K3 surfaces and the tetrahedron

Consider the quartic degeneration in $\mathbb{P}^3$

$$z_0 z_1 z_2 z_3 + t f_4(z_0, z_1, z_2, z_3) = 0.$$

For general f_4 and nonzero general t, the fiber is a smooth K3 surface. At $t = 0$ it is the union of the four coordinate planes, whose dual intersection complex is the boundary of a tetrahedron. The restriction of a general f_4 to each coordinate line has four zeros. These give 24 ordinary double points of the total space, with local equation $xy + tw = 0$. The corresponding integral affine model has four simple nodes on each of the six edges.

The integral affine charts. Take the lattice $N = \mathbb{Z}^3$ and the tetrahedron

$$P = \operatorname{Conv}\{p_0, p_1, p_2, p_3\}, \qquad B = \partial P,$$

$$p_0 = (-1, -1, -1), \quad p_1 = (3, -1, -1), \quad p_2 = (-1, 3, -1), \quad p_3 = (-1, -1, 3).$$

Each edge has integral length 4. Put one node at the midpoint of each of its four unit segments, and denote the resulting set of 24 nodes by Δ. The atlas on $B \setminus \Delta$ is as follows [14, §2.2]:

- A face interior carries the affine structure induced from its affine plane in $N_{\mathbb{R}}$.
- For each lattice point q on an edge, including the vertices, choose a small neighborhood $U_q \subset B \setminus \Delta$. Its chart is projection

  $$U_q \longrightarrow N_{\mathbb{R}}/\mathbb{R}q, \qquad \text{with lattice } N/\mathbb{Z}q.$$

  Along an edge, U_q ends at the adjacent nodes. Together with the face interiors, these neighborhoods cover $B \setminus \Delta$.

An incident facet has a primitive integral conormal n with $n(q) = 1$ or -1. Thus q is primitive and projection identifies that facet's tangent lattice with $N/\mathbb{Z}q$. The chart transitions are consequently integral affine, including near the tetrahedral vertices, which are regular points.

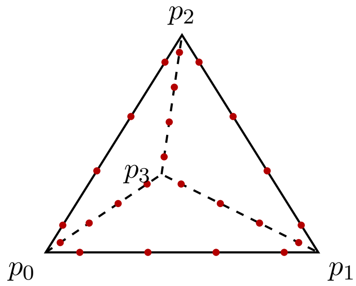

The affine tetrahedron. Red points are nodes; the tetrahedral vertices are regular. Dashed edges indicate the perspective projection.

For an explicit transition calculation, use coordinates (X, Y, Z) on $N_{\mathbb{R}}$ and consider the edge $Y = Z = -1$. Its lattice points are $q_r = (r-1, -1, -1)$, $r = 0, \dots, 4$. Quotient coordinates for the chart at q_r are

$$\chi_r(X, Y, Z) = \big(X + (r-1)Y,\ Z - Y\big).$$

On the two components of the overlap of consecutive charts,

$$\chi_{r+1} \circ \chi_r^{-1}(\xi, \eta) = \begin{cases} (\xi - 1, \eta), & \text{on the face } Y = -1, \\ (\xi - \eta - 1, \eta), & \text{on the face } Z = -1. \end{cases}$$

Going around the intervening node therefore gives the shear $(\xi, \eta) \mapsto (\xi - \eta, \eta)$, or its inverse according to loop orientation. Each node is a simple focus–focus singularity. The shear fixes the edge direction, and the four nodes on an edge give a shear of size 4 in total.

The 20 symplectic parameters. Let X be a marked symplectic K3 surface with a Lagrangian torus fibration and a Lagrangian section. Write $F, S \in H_2(X; \mathbb{Z})$ for the fiber and section classes, with orientations such that

$$F^2 = 0, \qquad F \cdot S = 1, \qquad S^2 = -2.$$

Thus $U = \langle F, S + F \rangle$ is a hyperbolic plane in the K3 lattice. The Lagrangian conditions give two independent equations

$$\int_F \omega = \int_S \omega = 0.$$

Since $b_2(X) = 22$, the local symplectic period space has real dimension $22 - 2 = 20$: its parameters lie in

$$\{\alpha \in U^\perp \otimes \mathbb{R} : \alpha^2 > 0\}, \qquad \operatorname{sign}(U^\perp) = (2, 18).$$

This includes overall scale. Locally these periods are realized by deforming an elliptic K3 with a holomorphic section and taking $\omega = \operatorname{Re}\Omega$; the holomorphic fibers and section are then Lagrangian. Nearby cohomologous symplectic forms are identified by Moser's argument. See [15, §§3.2.4, 6.7.1].

The matching affine count is 20 *modulo nodal slides*. A nodal slide moves a node along the invariant line of its local monodromy. Such slides change the fibration while preserving the underlying symplectic manifold [16, Proposition 6.2]. The full local space of integral affine spheres with 24 nodes has real dimension 44; its nodal-slide leaves have dimension 24. The local transverse space therefore has dimension $44 - 24 = 20$ [15, §6.7.1]. These are real symplectic and affine parameters.

Deforming the tetrahedral model. Here is the explicit calculation of these parameters. Label an edge by its endpoint indices ij, and label its four nodes by $r = 1, \ldots, 4$. At p_0, use quotient coordinates $\psi(X, Y, Z) = (X - Z, Y - Z)$. Developing the three incident face interiors through this chart places the vertices at

$$p_0 \mapsto (0,0), \quad p_1 \mapsto (4,0), \quad p_2 \mapsto (0,4), \quad p_3 \mapsto (-4,-4).$$

Choose cuts and based meridians through these faces. The transported primitive invariant directions, up to sign, are the edge directions in this development. In cyclic order they are

$$\begin{array}{c|cccccc} e & 01 & 12 & 02 & 23 & 03 & 13 \\ \hline v_e & (1,0) & (1,-1) & (0,1) & (1,2) & (1,1) & (2,1). \end{array}$$

With det the standard oriented determinant, put

$$M_v(x) = x + \det(v, x)v.$$

Writing $M_e = M_{v_e}$ and choosing the meridian orientation accordingly, the ordered product of the 24 linear monodromies is

$$M_{01}^4 M_{12}^4 M_{02}^4 M_{23}^4 M_{03}^4 M_{13}^4 = I.$$

If a developed node is at $b_{e,r}$, its affine monodromy is

$$T_{e,r}(x) = b_{e,r} + M_{v_e}(x - b_{e,r}).$$

Move it by $\epsilon u_{e,r}$ and set

$$t_{e,r} = \det(v_e, u_{e,r}), \qquad S_e = \sum_{r=1}^{4} t_{e,r}.$$

The change in the translation part of $T_{e,r}$ is $-\epsilon t_{e,r} v_e$. Motion parallel to v_e is invisible to this translation part: it is the nodal-slide direction.

The product of the affine monodromies must still be the identity. Multiplying in the above order gives the two equations

$$\begin{pmatrix} 1 & -3 & -8 & 5 & -7 & 2 \\ 0 & -1 & -3 & 2 & -3 & 1 \end{pmatrix} \begin{pmatrix} S_{01} \\ S_{12} \\ S_{02} \\ S_{23} \\ S_{03} \\ S_{13} \end{pmatrix} = 0.$$

Equivalently,

$$\begin{aligned} S_{01} - S_{12} - 2S_{02} + S_{23} - S_{03} &= 0, \\ S_{01} + S_{02} - S_{23} + 2S_{03} - S_{13} &= 0. \end{aligned} \tag{7}$$

These are two independent compatibility conditions. For example, choose the four sums S_{01}, S_{02}, S_{03} and S_{23} freely; then

$$\begin{aligned} S_{12} &= S_{01} - 2S_{02} + S_{23} - S_{03}, \\ S_{13} &= S_{01} + S_{02} - S_{23} + 2S_{03}. \end{aligned}$$

For each edge, distributing its sum among four nodes gives another three parameters. Thus there are $6 \cdot 3 + 4 = 22$ transverse parameters before changing the origin of the developing plane. For sufficiently small deformations the node ordering and the chosen cut pattern persist; with the linear parts fixed, the translation equations are linear, so the same formulas describe small finite deformations.

A common translation of developing coordinates by ϵa changes

$$u_{e,r} \longmapsto u_{e,r} + a, \qquad t_{e,r} \longmapsto t_{e,r} + \det(v_e, a).$$

It supplies two coordinate redundancies. Consequently

$$\underbrace{24-2-2}_{\text{transverse affine parameters}} = 20, \qquad \underbrace{48-2-2}_{\text{all node-position parameters}} = 44.$$

The extra 24 parameters in the second count are nodal slides. In this way, the six edge sums have four independent parameters before the translation quotient, and two afterwards; the other 18 transverse parameters redistribute the sums within edges. Sweeping a fiber circle along a path in the base computes a symplectic period from its integral affine displacement. This is how the 20 affine parameters match the periods in $U^\perp$.

A transverse motion equivalent to nodal slides. Fix $a = (1,3)$ in the developing plane and use its Euclidean inner product to set, for every node on edge e,

$$s_e = -\frac{\langle a, v_e\rangle}{|v_e|^2} v_e, \qquad u_e = a + s_e.$$

Then s_e is parallel to v_e, whereas u_e is perpendicular to v_e. For example,

e	s_e	u_e
01	$(-1,0)$	$(0,3)$
12	$(1,-1)$	$(2,2)$

Start with the slide family whose developed nodes are $b_{e,r} + \epsilon s_e$, and translate its entire developing map by $g_\epsilon(x) = x + \epsilon a$. The nodes now appear at $b_{e,r} + \epsilon u_e$, so all their apparent motions are transverse. Nevertheless, for each ϵ this is the same affine structure as the slide family, because

$$(\mathrm{dev}, \rho) \longmapsto (g_\epsilon \circ \mathrm{dev},\ g_\epsilon \rho g_\epsilon^{-1})$$

is a change of developing coordinates. Here both the developing map and its holonomy are transformed. Conjugate holonomy alone does not determine the affine structure: nodal slides preserve holonomy while moving the singularities along their invariant lines.

9.3 The generic singularity: a vector and a covector

At a smooth point of the codimension-two discriminant, the elementary SYZ-base model is a focus–focus singularity times $\mathbb{R}^{n-2}$. Here is a coordinate-independent description of its integral affine structure. Let Λ be the lattice of integral tangent vectors at a nearby regular point. Choose primitive elements

$$v \in \Lambda, \qquad \alpha \in \Lambda^* = \mathrm{Hom}(\Lambda, \mathbb{Z}), \qquad \alpha(v) = 0.$$

For a chosen orientation of a small meridian around the discriminant, the linear monodromy is

$$M = I + v \otimes \alpha, \qquad M(w) = w + \alpha(w)v.$$

Thus α measures the component that produces the shear, and v is the direction of the shear. In particular,

$$\ker(M-I)=\ker\alpha,\qquad \operatorname{im}(M-I)=\mathbb{Z}v,\qquad (M-I)^2=0.$$

The orthogonality condition gives $\det M=1$ and $M^{-1}=I-v\otimes\alpha$. Reversing the meridian replaces M by M^{-1}; replacing (v,α) by $(-v,-\alpha)$ leaves M unchanged. The primitivity assumptions describe a simple node. A shear of multiplicity $k\geq 1$ has $M=I+k\,v\otimes\alpha$.

The affine charts. Work in an affine space A with translation space $\Lambda_{\mathbb{R}}=\Lambda\otimes\mathbb{R}$. Choose a point $b\in A$ and a lattice complement K such that $\ker\alpha=\mathbb{Z}v\oplus K$. Set

$$D=b+K_{\mathbb{R}},\qquad H=b+(\ker\alpha)_{\mathbb{R}},\qquad C_{\pm}=D+\mathbb{R}_{\geq 0}(\pm v).$$

Here D is the codimension-two discriminant, H is the invariant hyperplane, and $C_{\pm}$ are its two halves bounded by D. The affine shear

$$T_b(x)=x+\alpha(x-b)v$$

fixes H pointwise and has linear part M. Take the two chart domains $U_{\pm}=A\setminus C_{\pm}$. Their overlap has two components; glue them by

$$x\longmapsto\begin{cases}x, & \alpha(x-b)<0,\\ T_b(x), & \alpha(x-b)>0.\end{cases}$$

Adding D topologically gives the required singular affine model. Going around D crosses the two overlap components and produces M or M^{-1} according to orientation. This is the usual two-chart description of the focus–focus singularity, with $n-2$ unchanged directions [17, §2.2]. In adapted coordinates, $v=e_1$, $\alpha=e_2^*$ and $D=\{x_1=x_2=0\}$, so

$$T_b(x_1,x_2,x_3,\ldots,x_n)=(x_1+x_2,x_2,x_3,\ldots,x_n),$$

where b is taken as the origin. In dimension three, D is an edge of the discriminant: its tangent and v together span $\ker\alpha$. The pair (v,α) records the monodromy; the choice of D also specifies where the singularity lies in this model.

The dual lattice and the vanishing cycle. On Λ^* the monodromy is the inverse transpose:

$$M^{-T}(\beta)=\beta-\beta(v)\alpha.$$

For the action–angle model T^*B_0/Λ^*, we have $H_1(L_q;\mathbb{Z})=\Lambda_q^*$ for a regular fiber L_q; the primitive vanishing cycle is therefore α, up to sign. Thus one must distinguish tangent-lattice monodromy on the base from monodromy on the first homology of the torus fiber. Dualizing exchanges the roles of the vector and covector, with the sign displayed above.

9.4 Positive and negative vertices in dimension three

There are two basic trivalent vertices. In both cases the local base is a three-ball and the discriminant is a Y-shaped graph. Along an open leg the singular fiber is a once-pinched two-torus times S^1. The names *positive* and *negative* refer to the Euler characteristic $+1$ or -1 of the fiber over the vertex. We keep the convention that Λ is the integral tangent lattice of the base and $H_1(L;\mathbb{Z})=\Lambda^*$.

The positive vertex. The complex affine threefold is

$$X_+ = \{(z_1, z_2, z_3) \in \mathbb{C}^3 : z_1 z_2 z_3 \neq 1\},$$

with the standard symplectic form restricted from $\mathbb{C}^3$. An explicit Lagrangian torus fibration is

$$\begin{aligned} f_+ : X_+ &\longrightarrow \mathbb{R}^3, \\ z &\longmapsto \left(\log|z_1 z_2 z_3 - 1|, \frac{|z_1|^2 - |z_2|^2}{2}, \frac{|z_1|^2 - |z_3|^2}{2} \right). \end{aligned}$$

The last two functions generate a Hamiltonian T^2-action preserving $z_1 z_2 z_3$, so all three functions Poisson commute. At a regular value their common level set is a compact three-torus. Writing the base coordinates as (s, a, b), the critical values are

$$\Delta_+ = \{(0, -r, 0) : r \geq 0\} \cup \{(0, 0, -r) : r \geq 0\} \cup \{(0, r, r) : r \geq 0\}.$$

Indeed, critical points have at least two of the z_i equal to zero. At the vertex the fiber is

$$L_+ \cong (T^2 \times S^1)/(T^2 \times \{\mathrm{pt}\}), \qquad \chi(L_+) = 1.$$

See [18, §3.4]. The integral affine coordinates on the regular base are action integrals; the displayed coordinates (s, a, b) are coordinates on the underlying base, with a, b already action coordinates.

In the notation of the previous section, the positive affine vertex has one common shear vector:

$$M_i = I + v \otimes \alpha_i, \qquad \alpha_i(v) = 0, \qquad \alpha_1 + \alpha_2 + \alpha_3 = 0.$$

Here v is primitive and α_1, α_2 form a lattice basis of $\mathrm{Ann}(v)$. After choosing a basis and meridians, we may write

$$M_1^+ = I + E_{12}, \qquad M_2^+ = I + E_{13}, \qquad M_3^+ = I - E_{12} - E_{13}.$$

Here E_{ij} is the elementary matrix. Their product is I. Their common fixed space in $\Lambda_{\mathbb{R}}$ is the line $\mathbb{R}v$, whereas their duals fix a plane in $H_1(L; \mathbb{R})$.

The negative vertex. The complex affine threefold is the conic bundle

$$X_- = \{(u, v, z_1, z_2) \in \mathbb{C}^2 \times (\mathbb{C}^*)^2 : uv = 1 + z_1 + z_2\}.$$

It is smooth, and its projection to $(\mathbb{C}^*)^2$ has a nodal conic over the pair of pants $\{1 + z_1 + z_2 = 0\}$. Evans–Mauri construct a Lagrangian torus fibration on this variety, with an exact symplectic structure obtained from an affine compactification, whose base is an open three-ball and whose discriminant is a Y-graph [19, §3.2].

Their construction first gives a contact-link fibration $g : M \to S^2$ with three exceptional values and contact form λ_M on M. On the complement of the skeleton Σ, Liouville flow gives

$$X_- \setminus \Sigma \cong \mathbb{R} \times M, \qquad \omega = d(e^t \lambda_M), \qquad F(t, m) = (t, g(m)).$$

Adding Σ as the central fiber gives the cone on S^2; its discriminant is the cone on the three exceptional values. The central fiber is a Lagrangian skeleton, with isotropic strata.

The central fiber is obtained by attaching a solid torus to $S^1 \vee S^1$. Up to homotopy, its attaching map sends the meridian to the commutator of the two circles and the longitude to the trivial loop [19, Theorem 3.4]. Consequently

$$\chi(L_-) = \chi(S^1 \vee S^1) + \chi(D^2 \times S^1) - \chi(T^2) = -1.$$

This also agrees with $\chi(X_-) = \chi(\{1 + z_1 + z_2 = 0\}) = -1$: the other conic fibers are $\mathbb{C}^*$ and contribute zero.

The negative affine vertex has one common shear covector:

$$M_i = I + v_i \otimes \alpha, \qquad \alpha(v_i) = 0, \qquad v_1 + v_2 + v_3 = 0,$$

where α is primitive and v_1, v_2 form a lattice basis of $\ker \alpha$. A choice dual to the positive matrices is

$$M_1^- = I - E_{21}, \qquad M_2^- = I - E_{31}, \qquad M_3^- = I + E_{21} + E_{31}.$$

Now the common fixed space in $\Lambda_{\mathbb{R}}$ is the plane $\ker \alpha$, while the common fixed space in $H_1(L; \mathbb{R})$ is a line. The discriminant can be drawn in this invariant plane. Each leg has the elementary shear from the previous section; its tangent lies in the relevant fixed plane and is distinct from its shear direction.

Thus the two bases have the same topological Y-shaped discriminant but different integral affine structures. Their monodromies satisfy

$$M_i^- = (M_i^+)^{-T},$$

which explains why dualizing the torus fibers exchanges the two vertex types. These statements concern the usual affine and Lagrangian models. In particular, the Y-shaped negative model above uses the Evans–Mauri construction; the Castaño-Bernard–Matessi construction instead has a small thickening of the discriminant near the negative vertex [18, §3.3].

9.5 Gross's SYZ base for the quintic threefold

Consider the degeneration

$$z_0 z_1 z_2 z_3 z_4 + t f_5(z_0, \ldots, z_4) = 0 \quad \text{in } \mathbb{P}^4$$

whose central fiber consists of five coordinate hyperplanes. In the moment-polytope picture, the five components contribute five tetrahedra, glued along their triangular faces. The resulting base is

$$B = \partial P \cong S^3, \qquad P = \{x \in \mathbb{R}^4 : x_i \geq -1,\ x_1 + x_2 + x_3 + x_4 \leq 1\}.$$

This is the reflexive moment simplex for the anticanonical polarization of $\mathbb{P}^4$. Its edges have integral affine length 5. Components correspond to facets here; in the dual intersection complex they correspond to vertices.

The discriminant graph. Subdivide each of the ten triangular faces into 25 elementary lattice triangles, and draw the dual graph: put a vertex in each small triangle and join vertices across common sides. At the boundary of the large triangle, end the corresponding edges at the midpoints of the five unit segments on each side. There are 25 trivalent vertices in each face and five ends on each side.

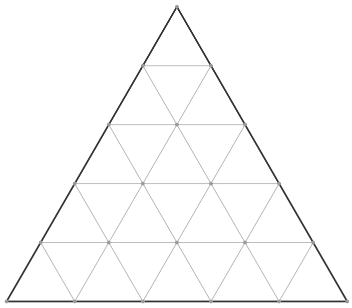

Degree-five triangle
25 unimodular triangles

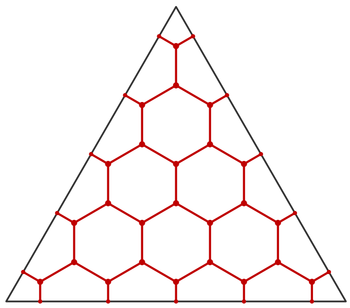

25 negative vertices
5 ends on each side; 6 cycles

Three triangular faces meet along every edge of the four-simplex. Identify their corresponding graph ends; this produces five trivalent vertices on each of the ten original edges. Let Δ be the resulting graph in B. Its vertices in face interiors are negative, and those on the original edges are positive. The original vertices of the four-simplex are regular points of the affine base.

The integral affine structure. Put $N = \mathbb{Z}^4$. Facet interiors inherit their affine lattices from N. For each lattice point q in the two-skeleton, take a suitable neighborhood $U_q \subset B \setminus \Delta$ and use the chart

$$U_q \longrightarrow N_{\mathbb{R}}/\mathbb{R}q, \qquad \text{with lattice } N/\mathbb{Z}q.$$

Choose U_q so that its intersection with the two-skeleton is the region around q bounded by the dual graph. These charts and the facet interiors cover $B \setminus \Delta$. As in the tetrahedral K3 model, an incident facet has primitive integral normal pairing ± 1 with q, so the projected tangent lattice is precisely $N/\mathbb{Z}q$. See [14, §2.4] for this affine atlas.

Using these charts, the local models along edges and at vertices of Δ are exactly those of the preceding two sections. The count is

$$\#V_- = 10 \cdot 25 = 250, \qquad \#V_+ = 10 \cdot 5 = 50.$$

Regular fibers and fibers over open graph edges have Euler characteristic zero. Thus the singular fibers give

$$\chi(X) = \#V_+ - \#V_- = 50 - 250 = -200,$$

as required for a smooth quintic.

Gross compactifies the regular torus bundle over this base to a topological torus fibration whose total space is diffeomorphic to a smooth quintic [20, §4, Theorem 4.1]. The compactified dual fibration is a smooth mirror quintic: the two vertex types exchange, and the Euler characteristic becomes $+200$. This is a topological SYZ construction; the assertion here does not include special Lagrangian fibers for a Ricci-flat metric.

9.6 Ray diagram bases for affine log Calabi–Yau surfaces

We now describe the bases constructed in [21]. A *rational ray diagram* $\mathcal{R}$ is a finite collection of rational rays $\rho_i = \mathbb{R}_{\geq 0} v_i \subset \mathbb{R}^2$, where $v_i \in \mathbb{Z}^2$ is primitive, together with multiplicities $m_i \in \mathbb{Z}_{\geq 0}$. On ρ_i choose m_i distinct points

$$b_{i,j} = r_{i,j} v_i, \qquad r_{i,j} > 0.$$

These will be simple focus–focus nodes. Draw a branch cut $b_{i,j} + \mathbb{R}_{\geq 0} v_i$ from each node outwards. The complement of these cuts carries the standard affine chart. Extend across them using the focus–focus charts, with invariant direction v_i and the convention that a straight affine geodesic, when drawn in the reference chart, bends towards the node as it crosses a cut. The resulting nodal integral affine plane is denoted $B_{\mathcal{R}}$ [21, Definition 1.7 and §1.1.1].

The elementary shear has the form

$$w \longmapsto w + \det(v_i, w)v_i$$

for one orientation of the meridian; reversing the orientation gives its inverse. The special feature is that every invariant line passes through the origin. This is an *exact eigenray diagram*. The positions $r_{i,j}$ are auxiliary: they are not part of $\mathcal{R}$.

The symplectic manifold. Over the regular part of $B_{\mathcal{R}}$ take the action–angle bundle $T^*B_{\mathcal{R}}^{\mathrm{reg}}/\Lambda^*$ and fill in the standard nodal fibers. The radial vector field $x_1\partial_{x_1} + x_2\partial_{x_2}$ in the reference chart extends over the regular affine base, since the transition shears fix the origin. Its horizontal lift is Liouville. Modifying this lift near the nodal fibers and completing gives a complete finite-type Liouville manifold $U_{\mathcal{R}}$.

Different choices, including the positions of the nodes, give strongly exact symplectomorphic $U_{\mathcal{R}}$ [21, Proposition 1.9]. Here the construction supplies Liouville deformations for the auxiliary choices, and §3.4 converts them into strongly exact symplectomorphisms. The affine bases and fibrations themselves can change under these choices. Equip $U_{\mathcal{R}}$ with the unique homotopy class of grading structures for which the regular torus fibers have Maslov class zero.

Obtaining the diagram from an affine surface. In dimension two every affine log Calabi–Yau surface admits a generalized toric model in the sense defined earlier [21, Theorem 2.1]. The symplectic conclusion is:

Theorem 9.1 (Ray diagram model, [21, Theorem 1.12])**.** *Every affine log Calabi–Yau surface U has an associated rational ray diagram $\mathcal{R}$ and a grading-preserving strongly exact symplectomorphism*

$$U_{\mathcal{R}} \simeq \widehat{U}.$$

The diagrams can be chosen by the following recipes.

If U is a *Looijenga interior*, so the boundary has nodes, choose a toric model without the boundary-smoothing step. Take the rays of the fan of its Toric Start, with multiplicity equal to the number of non-toric blowups on the corresponding boundary component. The determinant pairing identifies the fan lattice with the lattice used in the base diagram. Rays of multiplicity zero carry no nodes.

If the boundary is smooth, U is of *elliptic type*. There are ten deformation types, and the paper gives the following diagrams:

U	primitive ray directions	multiplicities
$\mathbb{P}^1 \times \mathbb{P}^1 \setminus D_{2,2}$	$(1,1), (1,-1), (-1,1), (-1,-1)$	$1,1,1,1$
$Y_d \setminus D, \quad d = 1, \ldots, 9$	$(1,0), (7,1), (-41,-5), (2d-17,-2)$	$9-d, 1, 1, 1$

Here Y_d is the degree-d del Pezzo surface obtained by blowing up $9-d$ points of $\mathbb{P}^2$, and D is a smooth anticanonical curve. The first row is the other degree-eight case. In the second row there are $12-d$ nodes; for $d = 9$ the first ray has multiplicity zero.

The construction starts with a moment polygon, realizes non-toric blowups by Symington surgeries, and realizes boundary smoothings by nodal trades. Nodal slides and branch moves arrange the invariant lines through one point. Symplectic Torelli for log Calabi–Yau surfaces then identifies the resulting compactification with the algebraic one; comparison of the Liouville primitives gives the strongly exact statement above. Deformation stability handles the auxiliary choices once such a family has been constructed; the comparison with the given algebraic surface also uses this Torelli and primitive comparison input. The elliptic recipes use a square in the first case and a mutated $\mathbb{P}^2$ triangle in the second [21, §§2.3–2.4].

9.7 The base for $\mathbb{P}^3$ minus a quartic K3 surface

Let $Q \subset \mathbb{P}^3$ be a smooth quartic and put $X = \mathbb{P}^3 \setminus Q$. This is affine log Calabi–Yau by ampleness and adjunction. We use the following refined tetrahedral model for its SYZ base. The identification of the completed symplectic realization of this model with $\widehat{X}$ is the geometric assumption for this example.

Take the $\mathcal{O}(4)$ moment tetrahedron

$$\Delta = \mathrm{Conv}\{(-1,-1,-1),(3,-1,-1),(-1,3,-1),(-1,-1,3)\}, \qquad o = 0.$$

The diagram below refines the left-hand model in [22, Example 9.1 and Figure 9.1]. Each of its six coarse negative vertices, with an outgoing leg of multiplicity four, is split into four simple negative vertices.

The discriminant. Put one positive vertex on each segment from o to a vertex of Δ. For each tetrahedral edge E, work in the triangular sheet $\mathrm{Conv}(o, E)$. Connect its two positive vertices by a chain containing four negative vertices. From each negative vertex, draw an outward radial leg to E. The four endpoints on E are the midpoints of its four unit lattice segments. Thus

$$\Gamma \subset \mathrm{Cone}_o(\mathrm{Skel}_1(\partial\Delta)), \qquad \#V_+ = 4, \qquad \#V_- = 6 \cdot 4 = 24.$$

The positive vertices have one incident branch for each of the three edges meeting at the corresponding tetrahedral vertex. Each negative vertex has two chain branches and one outward branch.

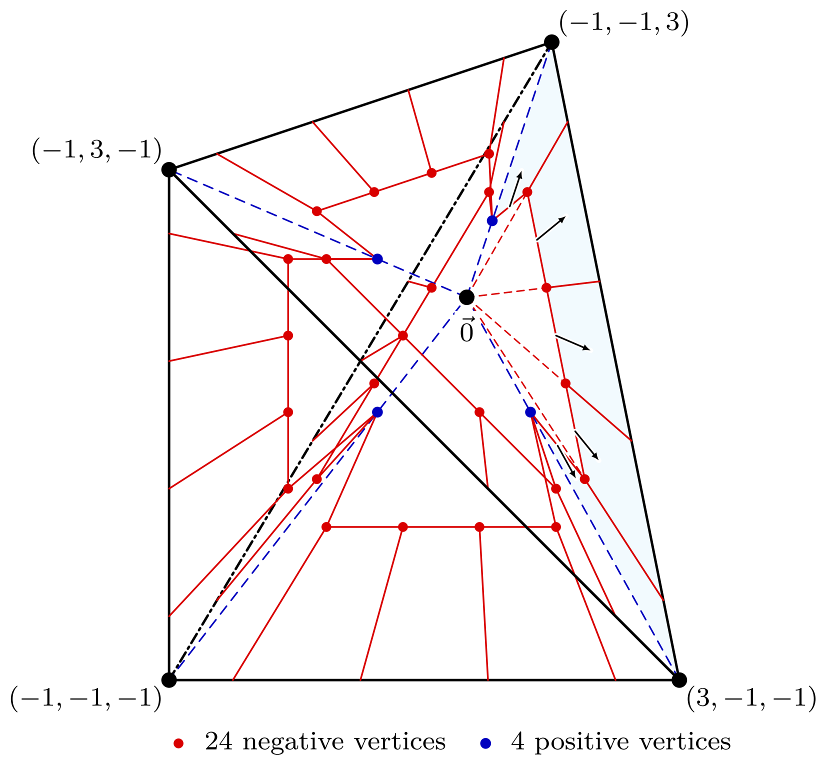

$\Gamma \subset \mathrm{Cone}_o(\mathrm{Skel}_1(\partial\Delta))$

The blue dashed lines are the radial edges of the star subdivision. The red solid graph is the discriminant. The red dashed segments from o to the four negative vertices on the displayed sheet are auxiliary radial continuations. Only the part of that sheet outside the discriminant chain is shaded. The black arrows record the five shear vectors described below.

The tetrahedron displays the compact part of the model. The outward legs continue into the end in the completed picture; extending the affine and symplectic structures into that end is part of the completed-model construction.

Reading the monodromy arrows. We interpret the black arrows using the tangent-lattice convention of §9.3. Orient a tetrahedral edge from a_0 to a_4 and write

$$e_E = \frac{a_4 - a_0}{4}, \qquad a_k = a_0 + k e_E, \quad k = 0, \ldots, 4.$$

Let ℓ_1, ℓ_2 be the primitive integral normals of the two adjacent facets, with facet equations $\ell_r(x) = 1$, and set $\alpha_E = \ell_2 - \ell_1$. This is a primitive integral covector vanishing on the plane spanned by a_0 and e_E. Cut along the five outer regions between the chain and E. Across the k-th region glue the standard affine charts by

$$M_k = I + a_k \otimes \alpha_E.$$

These transformations fix the sheet pointwise. They also make the boundary locally flat away from the outgoing discriminant legs: since $\ell_1(a_k) = 1$, we have $\ell_1 \circ M_k = \ell_2$. They give the monodromy around the five successive chain segments, with compatible choices of meridians. The four outward legs have shear vector e_E:

$$M_{\mathrm{rad}} = I + e_E \otimes \alpha_E, \qquad M_{k-1} M_k^{-1} M_{\mathrm{rad}} = I.$$

The relation follows from $a_{k-1} - a_k + e_E = 0$. Thus at a negative vertex the three shears share the covector α_E, exactly as in §9.4. At a positive vertex they share the vector given by the corresponding tetrahedral vertex.

For the shaded sheet in the figure,

$$\begin{aligned} a_0 &= (3,-1,-1), & e_E &= (-1,0,1), \\ a_k &= (3-k,-1,k-1), & \alpha_E(x) &= x_1+2x_2+x_3. \end{aligned}$$

These are precisely the five displayed arrow directions. They are shear vectors in the base lattice. On fiber homology the monodromy is instead

$$\beta \longmapsto \beta - \beta(a_k)\alpha_E, \qquad \beta \in \Lambda^*,$$

so the vanishing-cycle direction is α_E, up to sign.

The 24 points where the outgoing legs meet the boundary are focus–focus nodes of the induced integral affine sphere, as expected for the quartic K3 surface. The origin and the tetrahedral vertices are regular points of the affine model.

Finally, the vertex count gives the expected Euler characteristic

$$4 - 24 = -20 = \chi(\mathbb{P}^3) - \chi(Q).$$

The completed base has an end carrying the outgoing discriminant legs, rather than the closed three-sphere of the quintic example.

9.8 Batyrev, Harder, and Prince

Batyrev's construction starts with a reflexive lattice polytope and its polar dual. The associated toric varieties carry anticanonical hypersurface families that form candidate mirror pairs [23]. In dimension four for the polytope, suitable crepant resolutions give Calabi–Yau threefolds. This includes the toric starting point for the quintic example.

Harder's construction for toric weak Fano threefolds uses the pencil spanned by a general anticanonical divisor and the toric boundary on the dual toric side. One resolves its base curves by successive blowups and removes the fiber at infinity, obtaining a proper Landau–Ginzburg model [24, §5.2].

Prince develops integral affine and topological torus-fibration models for the 105 deformation families of smooth Fano threefolds [25]. These give a source of explicit bases and discriminant loci. The geometric identifications and HMS statements for such models are separate questions; we use the models to organize the examples that motivate the categorical framework.

In Lecture 3 we will turn from this geometric and categorical outline to the Floer constructions, especially the additional structure provided by support conditions.

References

[1] P. Seidel, *Graded Lagrangian submanifolds*, Bulletin de la Société Mathématique de France **128** (2000), 103–149. Available online.

[2] J. Milnor, *Spin structures on manifolds*, L'Enseignement Mathématique **9** (1963), 198–203. doi:10.5169/seals-38784.

[3] D. Auroux, *A beginner's introduction to Fukaya categories*. arXiv:1301.7056.

[4] K. Fukaya, Y.-G. Oh, H. Ohta, and K. Ono, *Antisymplectic involution and Floer cohomology*, Geometry & Topology **21** (2017), 1–106. doi:10.2140/gt.2017.21.1.

[5] P. Seidel, *A biased view of symplectic cohomology*, Current Developments in Mathematics **2006** (2008), 211–253. arXiv:0704.2055.

[6] K. Cieliebak and Y. Eliashberg, *Flexible Weinstein manifolds*. arXiv:1305.1635.

[7] K. Cieliebak and Y. Eliashberg, *From Stein to Weinstein and Back: Symplectic Geometry of Affine Complex Manifolds*, AMS Colloquium Publications **59** (2012), §11.2. Author version.

[8] T. de Fernex, J. Kollár, and C. Xu, *The dual complex of singularities*. arXiv:1212.1675.

[9] T. Perutz and N. Sheridan, *Constructing the relative Fukaya category*. arXiv:2203.15482.

[10] S. Bosch, *Lectures on Formal and Rigid Geometry*, lecture notes (2008). Available online.

[11] P. Seidel, *Fukaya A_∞-structures associated to Lefschetz fibrations. II*. Available online.

[12] J. J. Duistermaat, *On global action-angle coordinates*, Communications on Pure and Applied Mathematics **33** (1980), 687–706. doi:10.1002/cpa.3160330602.

[13] N. Martynchuk, H. W. Broer, and K. Efstathiou, *Hamiltonian monodromy and Morse theory*, Communications in Mathematical Physics **375** (2020), 1373–1392. arXiv:1901.00705.

[14] D. Matessi, *On real Calabi–Yau threefolds twisted by a section*, Journal of the London Mathematical Society **109** (2024), e12845. doi:10.1112/jlms.12845.

[15] M. Kontsevich and Y. Soibelman, *Affine structures and non-archimedean analytic spaces*. arXiv:math/0406564.

[16] M. Symington, *Four dimensions from two in symplectic topology*. arXiv:math/0210033.

[17] M. Gross and B. Siebert, *An invitation to toric degenerations*. arXiv:0808.2749.

[18] R. Castaño-Bernard and D. Matessi, *Conifold transitions via affine geometry and mirror symmetry*, Geometry & Topology **18** (2014), 1769–1863. arXiv:1301.2930.

[19] J. D. Evans and M. Mauri, *Constructing local models for Lagrangian torus fibrations*, Annales Henri Lebesgue **4** (2021), 537–570. arXiv:1905.09229.

[20] M. Gross, *Topological mirror symmetry*. arXiv:math/9909015.

[21] U. Varolgüneş, *Homological mirror symmetry for affine log Calabi–Yau surfaces*. arXiv:2608.13779.

[22] M. Carl, M. Pumperla, and B. Siebert, *A tropical view on Landau–Ginzburg models*, Acta Mathematica Sinica, English Series **40** (2024), 329–382. arXiv:2205.07753.

[23] V. V. Batyrev, *Dual polyhedra and mirror symmetry for Calabi–Yau hypersurfaces in toric varieties*. arXiv:alg-geom/9310003.

[24] A. Harder, *Hodge numbers of Landau–Ginzburg models*. arXiv:1708.01174.

[25] T. Prince, *Lagrangian torus fibration models of Fano threefolds*. arXiv:1801.02997.

[26] J. Kollár and C. Xu, *The dual complex of Calabi–Yau pairs*. arXiv:1503.08320.

[27] M. F. Tehrani, M. McLean, and A. Zinger, *Normal crossings singularities for symplectic topology*. Available online.

[28] V. Drinfeld, *DG quotients of DG categories*, Journal of Algebra **272** (2004), 643–691. arXiv:math/0210114.